39th AIAA/ASME/SAE/ASEE Joint Propulsion Conference and Exhibit
20-23 July 2003, Huntsville, Alabama

AIAA 2003-4429

NOZZLE PERFORMANCE OF A RP LASER THRUSTER

Yasuro Hirooka*, Hiroshi Katsurayama†, Koichi Mori‡, Chihiro Inoue*,
Kimiya Komurasaki§ and Yoshihiro Arakawa¶
The University of Tokyo, Hongo 7-3-1, Bunkyo, Tokyo 113-8656, Japan

Abstract

In order to reveal the nozzle scaling law of a Repetitive Pulsed (RP) laser thruster, momentum-coupling coefficients of several conical nozzles were investigated by means of experiment and numerical analysis. In the experiment, a pendulum method was used to measure an impulse imparted to a conical nozzle by a laser-driven blast wave. A propagation of the blast wave in a conical nozzle and an exhaust-refill process were analyzed by CFD. The calculated C_m agreed with the experimental data. The processes until a critical time are qualitatively the same regardless of a divergence angle, but quantitatively different. As a result, the nozzle of a small apex angle enhances the performance of a RP laser thruster when only a single pulse is input.

INTRODUCTION

A RP laser thruster is attracting attention as a low-cost launching system recently.

A RP laser thruster is free from on-board energy sources because laser beam is transmitted from laser bases on the earth or space. In addition, it can use an ambient atmosphere as a propellant until it reaches very high altitudes. Thereby, a RP laser thruster will increase its payload ratio drastically in comparison with conventional chemical propulsion rockets.

A RP laser thruster generates thrust by following mechanisms. The plasma produced by laser focusing expands rapidly, and its expansion drives a high-pressure blast wave. The blast wave imparts an impulse directly to a nozzle wall and is accelerated aerodynamically through the nozzle.

Momentum coupling coefficient C_m is defined as,

$$C_{\mathrm{m}} = \frac{I}{E_{\mathrm{i}}}, \qquad (1)$$

where I is the impulse and E_{i} is the input laser energy.

E_{i} is converted to I through the sequential processes (a)-(d) shown in Fig.1. In the process (a), the plasma absorbs the input laser energy in the form of a Laser Supported Detonation (LSD) wave or a Laser Supported Combustion (LSC) wave.

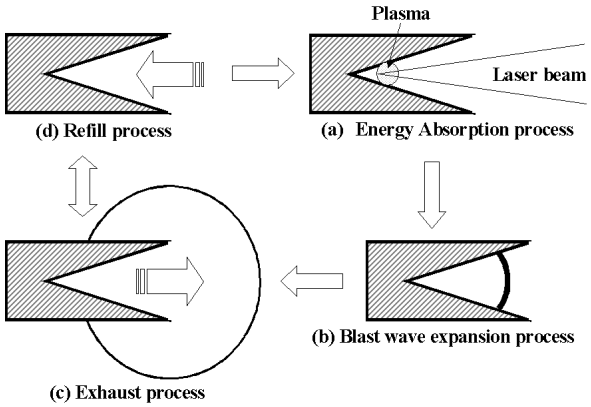

Fig.1 Conversion processes from E_{i} to I

In the process (b), the absorbed energy is converted to blast wave energy E_{bw}, chemical potential energy and radiation energy. E_{bw} is defined as,

$$E_{\mathrm{bw}} = \int [\rho e^{\mathrm{t+r}}(T) + \frac{\rho(u^2+v^2)}{2} - \rho_0 e^{\mathrm{t+r}}(T_0)]dV \ , \qquad (2)$$

where

$$\rho e^{\mathrm{t+r}} = \sum_{s=1}^{11} \rho_{\mathrm{s}} \left[\int C_{\mathrm{V}}^{\mathrm{s}}(T)dT - \int C_{\mathrm{V,V}}^{\mathrm{s}}(T)dT - \Delta e_{\mathrm{s}}^{\mathrm{f}} \right]. \qquad (3)$$

The subscript 0 indicates the properties before laser incidence and s indicates species. ρ is density, $e^{\mathrm{t+r}}$ is the sum of translational and rotational energies, T is static temperature, u, v are axial, radial velocity components respectively, $C^{\mathrm{s}}_{\mathrm{V}}$ is specific heat at constant volume for species s, $C^{\mathrm{s}}_{\mathrm{V,V}}$ is specific heat at constant volume for species s for vibrational energy, and Δe^{f} is

* Graduate student, Department of Aeronautics and Astronautics
† Graduate student, Department of Aeronautics and Astronautics, Student Member AIAA
‡ Graduate student, Department of Advanced Energy, Student Member AIAA
§ Associate Professor, Department of Advanced Energy, Member AIAA
¶ Professor, Department of Aeronautics and Astronautics, Member AIAA

chemical potential energy.

The following η_{bw}, is defined to investigate the conversion from E_i to E_{bw} in a RP laser thruster.

$$\eta_{bw} = \frac{E_{bw}}{E_i}. \quad (4)$$

The conversion process from E_i to E_{bw} has been discussed in our previous research.[1)]

In the processes (c) and (d), the blast wave energy is converted to the impulse through the nozzle. Since these processes control an exhaust-refill of air, the clarification of these processes is indispensable to predict a performance of a RP laser thruster.

The objective of this paper is to reveal nozzle-scaling parameters sensitive to C_m qualitatively and quantitatively, taking a conical nozzle as an example.

The experiments using conical nozzles were conducted.[2)] They showed that exhaust and refill processes influence on C_m greatly. However, it is difficult to clarify these processes in detail by the experimental results.

In the present paper, the propagations of blast waves inside and outside of conical nozzles were reproduced by CFD, and the influence of the exhaust-refill process on C_m was investigated.

EXPERIMENTAL RESULTS

Blast wave energy conversion efficiency

A TEA CO_2 laser was used and E_i was changed from 2 to 11 J. The duration of the laser pulse was mostly 3 μs. The laser beam was focused using an off-axial parabola mirror.

Blast wave energy was calculated using the shadowgraph images of the laser-driven shock wave. The experimental apparatus and analysis methods are presented in our previous report.[1)] Figure 2 shows the relation between E_i and E_{bw}. The errors in E_{bw} were mostly attributed to the fluctuations in E_i. E_{bw} was proportional to E_i, and η_{bw} was found 0.47 ± 0.05. The efficiency was insensitive to the input laser energy within the tested range.

Experimental results with conical nozzles

The dependency of C_m on a half divergence angle α_d of a conical nozzle is shown in Fig.3. C_m became max when α_d is a minimum value, $10°$. C_m decreased exponentially with the increase in α_d.

The relation between C_m and the nozzle length is shown in Fig.4, where a scaling parameter r represents the nozzle length. r is defined as,

$$r = \frac{R_n}{R^*}, \quad (5)$$

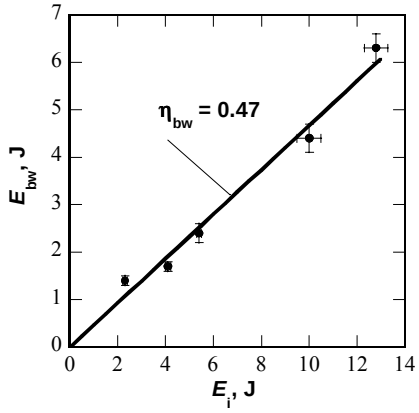

Fig.2 E_{bw} vs. E_i[2)]

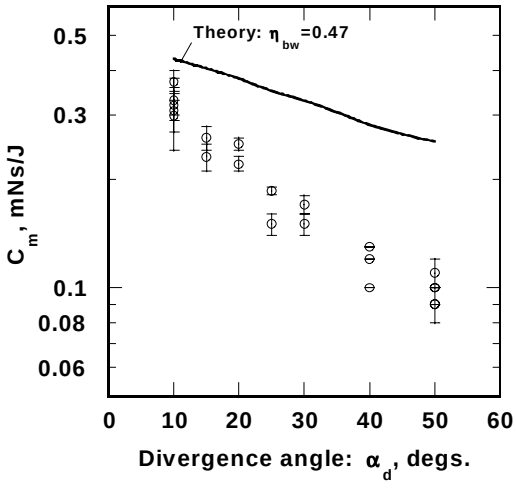

Fig.3 Influence of α_d on C_m[2)]

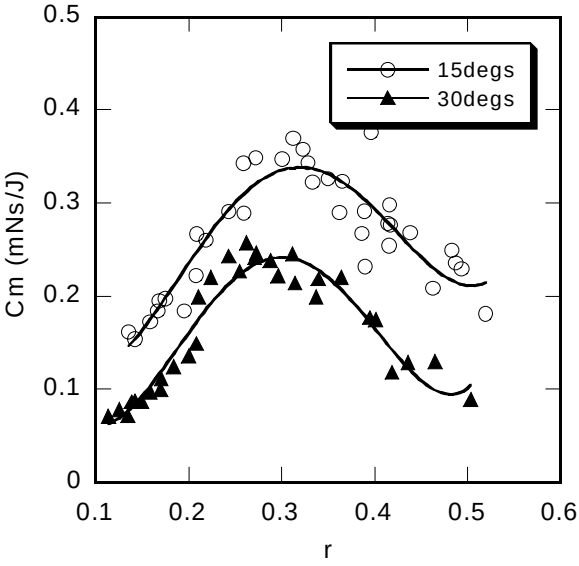

Fig.4 Influence of nozzle length on C_m[2)]

where R_n is an actual nozzle length and R^* is a characteristic radius of shock wave defined as,

$$R^* = \left(\frac{E_i / \sin^2(\alpha_d/2)}{p_a} \right)^{\frac{1}{3}}, \quad (6)$$

where p_a is an ambient pressure. R^* is a measure of the strength of explosion, and this is equivalent to the radius of the shock wave R_s when the pressure at the shock front decayed mostly to p_a .

In this measurement, five nozzles with different R_n were tested, and E_i was varied from 6 to 11 J for each nozzle. As a result, the influence of R_n and E_i on C_m can be expressed by the scaling parameter r.

C_m takes maximum value when r = 0.3 regardless of α_d, whereas the max C_m decreases with the increase in α_d. Thereby, α_d would influences the exhaust-refill process qualitatively and quantitatively.

COMPUTAIONAL METHOD

Governing equations

Axisymmetric Navier-Stokes equations are solved. Air is treated as an ideal gas. Then, the governing equations are given by

$$\frac{\partial \mathbf{U}}{\partial t} + \frac{\partial \mathbf{F}}{\partial z} + \frac{1}{r}\frac{\partial r\mathbf{G}}{\partial r} = \frac{\partial \mathbf{F_v}}{\partial z} + \frac{1}{r}\frac{\partial r\mathbf{G_v}}{\partial r} + \frac{\mathbf{H}}{r}, \quad (7)$$

$$\mathbf{U} = \begin{bmatrix} \rho \\ \rho u \\ \rho v \\ E \end{bmatrix}, \mathbf{F} = \begin{bmatrix} \rho u \\ \rho u^2 + p \\ \rho uv \\ (E+p)u \end{bmatrix}, \mathbf{G} = \begin{bmatrix} \rho v \\ \rho uv \\ \rho v^2 + p \\ (E+p)v \end{bmatrix},$$

$$\mathbf{F_v} = \begin{bmatrix} 0 \\ \tau_{zz} \\ \tau_{zr} \\ u\tau_{zz} + v\tau_{zr} + q_z \end{bmatrix}, \mathbf{G_v} = \begin{bmatrix} 0 \\ \tau_{zr} \\ \tau_{rr} \\ u\tau_{zr} + v\tau_{rr} + q_r \end{bmatrix},$$

$$\mathbf{H} = \begin{bmatrix} 0 \\ 0 \\ p - \tau_{\theta\theta} \\ 0 \end{bmatrix}. \quad (8)$$

E and the equation of state are defined as

$$E = \rho C_p T - p + \frac{\rho(u^2 + v^2)}{2}, \quad (9)$$

$$p = \rho RT, \quad (10)$$

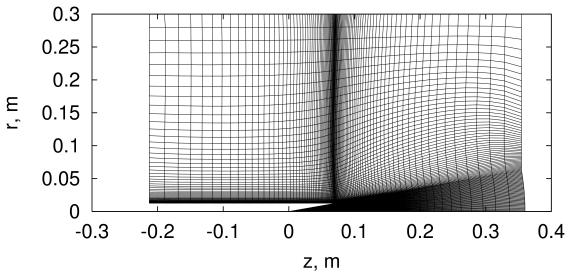

(a) Overall (12,005 cells)

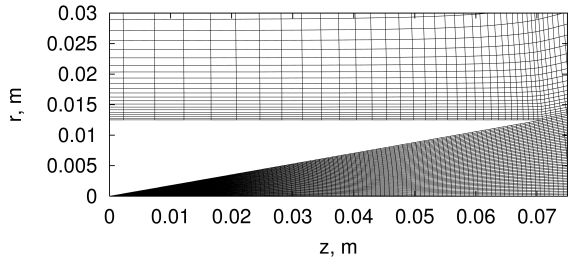

(b) Inside of nozzle (4,802 cells) and neighborhood

Fig.5 Computational meshes

$$C_p = \frac{\gamma}{\gamma - 1} R. \quad (11)$$

Specific heat ratio γ is 1.4 and gas constant of air R is 287 J/(K▪kg).

Transport properties are estimated using Southerland's equation.

Numerical Scheme

The blast wave expansion in a nozzle is computed by means of CFD. A cell-centered finite difference scheme is adopted. Inviscid flux is estimated with the AUSM-DV scheme[3] and space accuracy is extended to 3rd-order by the MUSCL approach with Edwards's pressure limiter[4]. Viscous flux is estimated with a standard central difference. Time integration is performed with the LU-SGS scheme[5] that is extended to 3rd-order time accuracy by Matsuno's inner iteration method[6]. The calculation is performed with the CFL number of 2 – 8.

The momentum transfer from blast wave to thrust is examined taking α_d as a parameter.

Computational mesh

Two sets of an apex angle and a nozzle length in Table 1 are used to clarify the dependency of C_m on these parameters. Both configurations have the same value of r in order to investigate the influence of α_d on C_m.

Figure 5 (a) shows computational meshes of a conical nozzle, the nozzle exit diameter and the half

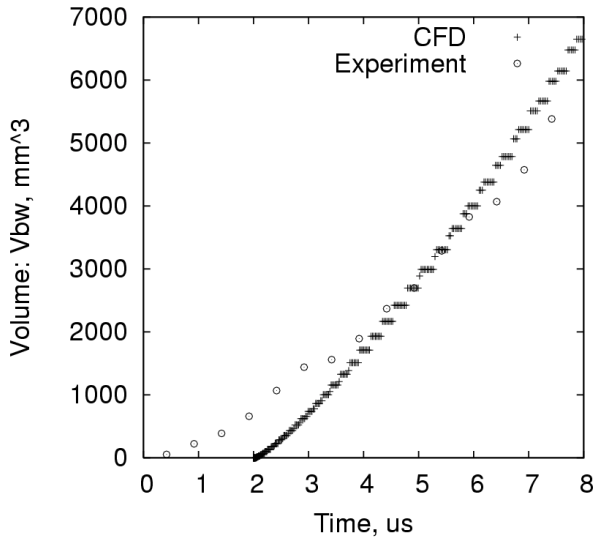

Fig.6 Comparison of CFD and experiment on V_{bw} (E_i = 10 J, η_{bw} =0.47)

Table 1 Configuration of Calculation

α_d, degrees	10	30
R_n, mm	72.0	34.8
Nozzle exit radius, mm	12.5	17.4
r	0.306	0.306

apex angle of which are 25 mm and 10° , and the adjacent region.

Figure 5 (b) is an enlarged view of the nozzle. The mesh of inside of the nozzle is fine enough to correctly capture the propagation of a blast wave.

The outer boundary of the computational zone is set far from the nozzle to reduce the influence of non-physical reflection waves from the outer boundary.

Explosion source model

An explosion source model[7] is adopted instead of solving the LSD phenomenon using a thermo-chemically non-equilibrium model. The explosion source is modeled as a pressurized volume. Since the LSD process can be considered to be isometric heating[8], the density in the source is assumed to be equal to an ambient atmosphere.

In this paper, an explosion source was assumed to be a sphere. Its initial radius was set to 1 mm. η_{bw} in the source is taken from experimental data, η_{bw} =0.47. E_i is 10 J. η_{bw} and E_{bw} are constant at any moment due to the assumption of ideal gas.

It can be seen reasonable with Fig.6 to fix the initial source radius at 1 mm to reproduce the

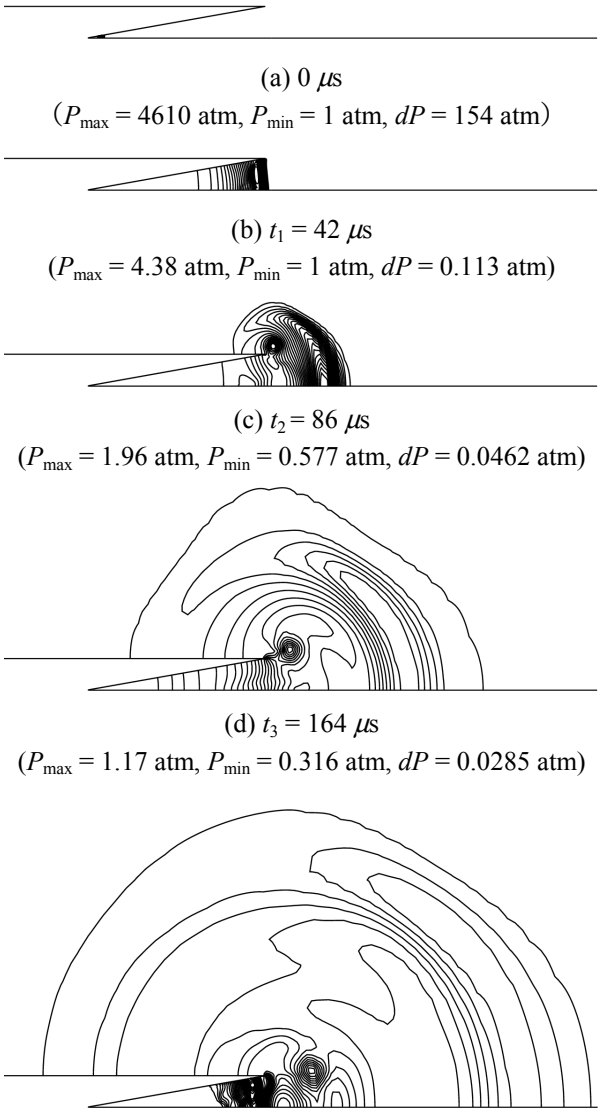

(a) 0 μs
(P_{max} = 4610 atm, P_{min} = 1 atm, dP = 154 atm)

(b) t_1 = 42 μs
(P_{max} = 4.38 atm, P_{min} = 1 atm, dP = 0.113 atm)

(c) t_2 = 86 μs
(P_{max} = 1.96 atm, P_{min} = 0.577 atm, dP = 0.0462 atm)

(d) t_3 = 164 μs
(P_{max} = 1.17 atm, P_{min} = 0.316 atm, dP = 0.0285 atm)

(e) t_4 = 288 μs
(P_{max} = 1.11 atm, P_{min} = 0.657 atm, dP = 0.0152 atm)

Fig.7 Pressure Contour (E_i=10 J, α_d = 10°)

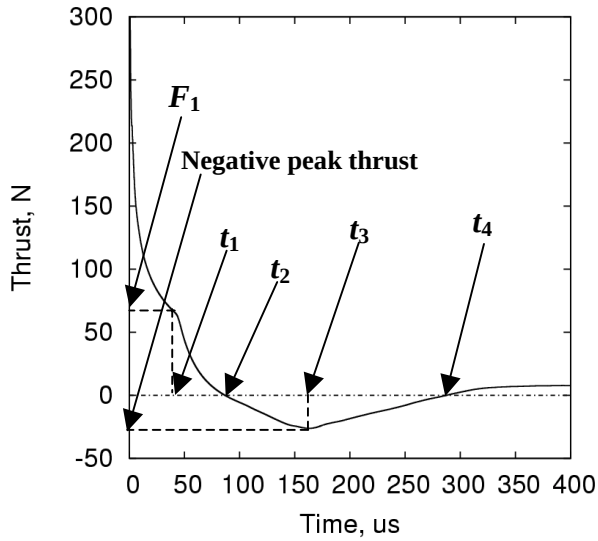

Fig.8 History of thrust (E_i=10 J, α_d = 10°)

exhaust-refill process. Figure 6 shows the histories of the volume of the driven blast wave, V_{bw}, in CFD and experiment. Although V_{bw} in CFD and experiment are different at early time because CFD neglects the heating process, V_{bw} in CFD agrees approximately with that in the experiment after 4 μs, when the laser-heating terminates.

The source was set so that it contacted the wall of a conical nozzle. In this case, its maximum position was 4.76 mm from the apex with α_d = 10° nozzle.

COMPUTATIONAL RESULTS

Blast waves were driven on the condition, E_i = 10J and η_{bw}=0.47. Figure 7 (a)-(e) show the pressure contours in the case of α_d = 10°. In Fig.7 (a), a highly pressurized source exits near the apex. In Fig.7 (b), a shock wave reaches the nozzle exit and a rarefaction wave is propagating in the direction of the apex.

Figure 8 is the history of the thrust. The maximum value of the thrust is over 800 N at t_0 = 0 μs, but the range over 300 N is omitted in the figure. The thrust decreases drastically until t_1 = 42 μs in Fig.7 (b). The thrust is kept to be positive until t_2 = 86 μs in Fig.7 (c), and then decreases to negative. The recovery from negative thrust starts at t_3 = 164 μs in Fig.7 (d), and the thrust again returns to positive at t_4 = 288 μs in Fig.7 (e). Pressure waves propagate very far from the nozzle exit at this time. After this time, the thrust periodically oscillates on zero thrust. Its oscillation attenuates gradually.

DISCUSSION

The history of C_m of CFD is compared with the experimental data in Table 2. Each total C_m agrees approximately although the numerical one is slightly lower than the experimental one. Thereby, the present CFD model can be reproduce the propagation process of the blast wave in the experiment.

The dependency of C_m on α_d is small at t_1. The tendency continues until t_3. However, after t_3, the C_m of α_d = 30° decreases more rapidly than that of α_d = 10°. The C_m decreased between $t_2 \sim t_4$ is recovered by only 15% after t_4 in the case of α_d = 30°. However, in the case of α_d = 10°, the recovery rate is 92 %. As a result, the total C_m in the case of α_d = 10° is much greater than that in the case of α_d = 30°. Thereby, when α_d is small, C_m is especially dependent on the exhaust-refill process after the shock wave has propagated far from the nozzle exit.

Table 2 Comparison of CFD and experiment on C_m

		C_m, N/MW	
α_d, degrees		10	30
CFD	~t_1	466	450
	~t_2	582	556
	~t_3	465	444
	~t_4	300	221
	Total	452	255
Experiment		462	259

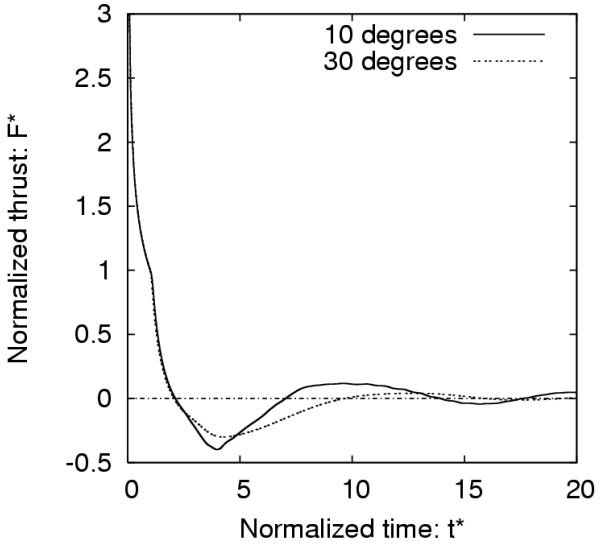

Fig.9 History of normalized thrust (E_i=10 J)

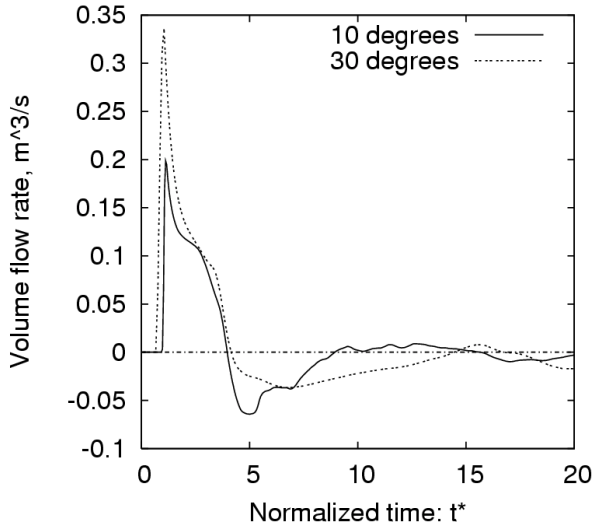

Fig.10 History of volume flow rate (E_i=10 J)

Figure 9 shows the history of normalized thrust. Its horizontal axis denotes normalized time t^*, defined as,

$$t^* = \frac{t}{t_1}, \tag{12}$$

and its vertical axis denotes normalized thrust F^*,

defined as,

$$F^* = \frac{F}{F_1}, \qquad (13)$$

where t is real time, F is the thrust at t and F_1 is the thrust at t_1. t_1 is about 41 μs in the case of $\alpha_d = 10°$ and about 21μs in the case of $\alpha_d = 30°$. Hence the time scale of $\alpha_d = 10°$ is in reality twice as long as that of $\alpha_d = 30°$. In the following discussion subscripts 1 ~ 4 of t^* mean the same states as in the previous section.

In any α_d, F^* decreases from positive to negative at $t^*_2 \cong 2\ t^*_1$ and its history is completely independent of α_d until approximately $t^*_c \cong 2.6\ t^*_1$. As a result, the qualitative aspect of the propagation of the blast wave is independent of α_d until t^*_c. However, after t^*_c, the history of F^* is dependent on α_d. The negative peak value of F^* decreases with α_d. On the other hand, the duration of the negative F^*, i.e. $t^*_4 - t^*_2$, increases with α_d. The exhaust is considered to be dominant in comparison with the refill until t^*_3. t^*_3 is almost equal regardless of α_d. After t^*_3, the refill is considered to take over the exhaust. Hence, the refill becomes less active with increase in α_d.

Figure 10 shows the history of volume flow rate at the nozzle exit. The gas is exhausted from the nozzle when the value of volume flow rate is positive and the gas is refilled into the nozzle when it is negative.

The exhaust volume increases rapidly when the shock front passes the nozzle exit, and reaches the maximum at about t^*_1. Then, it decreases drastically and the exhaust and refill are balanced at about t^*_3.

Then exhaust volume decreases drastically and the exhaust and refill are balanced at about t^*_3.

After t^*_3, the refill process becomes dominant and the change of volume flow rates is significantly different between two α_d. The refill process keeps dominant for almost the same period in both cases because the normalizing parameter t_1 of $\alpha_d = 10°$ is twice as long as that of $\alpha_d = 30°$. However, the normalized period for the refill process of $\alpha_d = 10°$ is twice as short as that of $\alpha_d = 30°$. Accordingly, a small α_d is found to prompt the refill process.

These exhaust and refill processes correspond to the history of normalized thrust.

From the above discussion, the nozzle of a small apex angle enhances the performance of a RP laser thruster when only a single pulse is input. However, since a RP laser thruster must receive multi laser pulses in a high frequency, the time scale of generating thrust is very important.

For example, if the refill process is enforced by an active method before t^*_c, C_m of $\alpha_d = 30°$ would be approximately twice as great as that of $\alpha_d = 10°$.

However, the real-duration of the exhaust-refill process after t^*_c is dependent on α_d. The causes should be further investigated.

SUMMARY

The propagation of blast wave in a conical nozzle and the exhaust-refill process were analyzed by CFD. The calculated C_m agreed with the experimental data.

The normalized thrusts of $\alpha_d = 10°$ and $30°$ agree almost completely until some critical time, however, differ each other after that time. This means that the phenomena until the critical time are qualitatively the same regardless of α_d, but quantitatively different. After that time, the refill process is more active in the case of $\alpha_d = 10°$ than in the case of $\alpha_d = 30°$. This causes that the recovery of C_m of $\alpha_d = 10°$ increases more greatly than that of $\alpha_d = 30°$ after the refill process becomes dominant. As a result, the nozzle of a small apex angle enhances the performance of a RP laser thruster when only a single pulse is input.

The duration of the exhaust-refill is also very important because a RP laser thruster must receive multi laser pulses in high frequency. For this reason, it is still not cleared whether a small apex nozzle is more appropriate for a RP laser thruster. The time scale of the exhaust and refill processes after the critical time must be further investigated.

REFERENCES

[1] Mori, K., Komurasaki, K., and Arakawa, Y., J. Appl. Phys. **9**2, 10, 2002

[2] Mori, K., Katsurayama, H., Hirooka, Y., Komurasaki K., and Arakawa, Y.: An Experimental Study on the Energy Balance in the Repetitively Pulsed Laser Propulsion, AIAA 2003-496.

[3] Wada, Y., and Liou, M.S.: A Flux Spliting Scheme With High-Resolution and Robustness for Discontinuities, NASA Technical Memorandum 106452 ICOMP-93-50, AIAA 94-0083.

[4] Edwards, J.R.: A Low-Diffusion Flux-Splitting Scheme for Navier-Stokes Calculations, Computers Fluids, 26, pp635-659, 1997

[5] Jameson A., and Yoon, S.: Lower-Upper Implicit Schemes with Multiple Grids for the Euler Equations, AIAA Journal, 25, pp929-935, 1987

[6] Matsuno, K.: Actual Numerical Accuracy of an Iterative Scheme for Solving for Solving Evolution Equations with Application to Boundary-Layer Flow, Trans. Japan Soc. Aero. Space. Sci., 38, pp.311-322, 1996

[7] Ritzel, D.V., and Matthews, K.: An adjustable explosion-source model for CFD blast calculations, Proc. Of 21st International Symposium on Shock Waves, pp.97-102, 1997

[8] Raizer, Y.P.: Laser-Induced Discharge Phenomena Studies in Soviet Science, Consultants Bureau, New York and London, 1977.